

# Real-Time Monitoring of the Oxalate Decarboxylase Reaction and Probing Hydron Exchange in the Product, Formate, Using Fourier Transform Infrared Spectroscopy<sup>†</sup>

Mylrajan Muthusamy,<sup>‡</sup> Matthew R. Burrell,<sup>‡</sup> Roger N. F. Thorneley, and Stephen Bornemann\*

Biological Chemistry Department, John Innes Centre, Norwich Research Park, Colney, Norwich NR4 7UH, United Kingdom

Received March 8, 2006; Revised Manuscript Received June 29, 2006

**ABSTRACT:** Oxalate decarboxylase converts oxalate to formate and carbon dioxide and uses dioxygen as a cofactor despite the reaction involving no net redox change. We have successfully used Fourier transform infrared spectroscopy to monitor in real time both substrate consumption and product formation for the first time. The assignment of the peaks was confirmed using [<sup>13</sup>C]oxalate as the substrate. The  $K_m$  for oxalate determined using this assay was 3.8-fold lower than that estimated from a stopped assay. The infrared assay was also capable of distinguishing between oxalate decarboxylase and oxalate oxidase activity by the lack of formate being produced by the latter. In D<sub>2</sub>O, the product with oxalate decarboxylase was C-deuterio formate rather than formate, showing that the source of the hydron was solvent as expected. Large solvent deuterium kinetic isotope effects were observed on  $V_{max}$  ( $7.1 \pm 0.3$ ),  $K_m$  for oxalate ( $3.9 \pm 0.9$ ), and  $k_{cat}/K_m$  ( $1.8 \pm 0.4$ ) indicative of a proton transfer event during a rate-limiting step. Semiempirical quantum mechanical calculations on the stability of formate-derived species gave an indication of the stability and nature of a likely enzyme-bound formyl radical catalytic intermediate. The capability of the enzyme to bind formate under conditions in which the enzyme is known to be active was determined by electron paramagnetic resonance. However, no enzyme-catalyzed exchange of the C-hydron of formate was observed using the infrared assay, suggesting that a formyl radical intermediate is not accessible in the reverse reaction. This restricts the formation of potentially harmful radical intermediates to the forward reaction.

Oxalate decarboxylase (EC 4.1.1.2) catalyzes the conversion of oxalate to carbon dioxide and formate (1, 2). The reaction involves no net redox change and yet dioxygen is required for catalysis (3–6). We identified Mn(II) to be the cofactor for both this enzyme (6) and oxalate oxidase (7) and proposed divergent catalytic mechanisms to rationalize their modes of action. Both of these oxalate-degrading enzymes are members of the cupin superfamily (8), and their Mn(II) coordination environments are very similar (9, 10). Oxalate decarboxylase has attracted a lot of attention recently because of the likely involvement of free radicals to cleave a relatively stable carbon–carbon bond and its apparent involvement in acid pH stress in *Bacillus subtilis* (11) and in regulation of lignin degradation (12) together with its potential commercial applications (13). Most effort has been in defining the catalytic cycle and reaction specificity using heavy atom isotope effects (14), electron paramagnetic resonance spectroscopy (15), density functional theory calculations (16), and homology modeling with oxalate oxidase sequences (17) together with crystallography and mutagenesis (10, 18). A key proposed catalytic intermediate is a manganese-bound formyl radical (Figure 1). We have

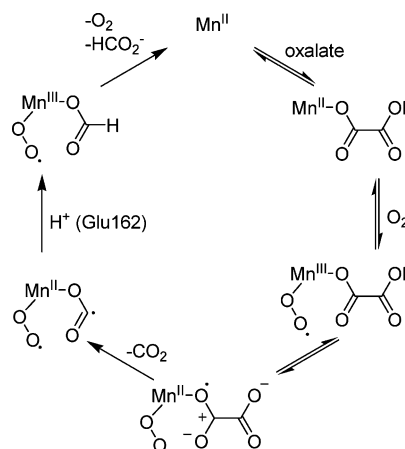


FIGURE 1: Proposed catalytic cycle of oxalate decarboxylase. Evidence for this scheme is described in the text.

presented evidence that such an intermediate is likely to be protonated by Glu162, leading to the formation of the product, formate (18). It is most likely that the source of the protons is ultimately solvent, but to our knowledge no direct evidence of this has been published. The  $pK_a$  of the proposed intermediate is expected to be relatively high. However, it is not known whether the enzyme lowers it sufficiently to allow the C-hydron to be exchanged when the enzyme is incubated with formate.

To address such mechanistic questions, a suitable assay for oxalate decarboxylase activity is required. Several methods have so far been described (19). A commonly used

<sup>†</sup> This research was supported by the Biotechnology and Biological Sciences Research Council with a Core Strategic Grant for the John Innes Centre and a Biochemistry & Cell Biology Committee Studentship for M.R.B.

\* Correspondence should be addressed to this author. Tel: +44 1603 450741. Fax: +44 1603 450018. E-mail: stephen.bornemann@bbsrc.ac.uk.

<sup>‡</sup> Contributed equally to this work.

approach has been to couple the production of formate to the reduction of NAD using formate dehydrogenase (20). This method is convenient, but the poor  $K_m$  of formate dehydrogenase for formate precludes a continuous assay. It is also possible to monitor the reaction in a stopped assay using [ $^{14}\text{C}$ ]oxalate and to measure the radioactivity in either the substrate (21) or products (10, 22). Another method uses nuclear magnetic resonance to monitor the  $^{13}\text{C}$  resonances of oxalate and formate (17). However, the sensitivity of this method precludes convenient real-time monitoring. Other stopped assays include those that monitor oxalate (23) and formate (24) using liquid chromatography. Other biochemical and chemical methods for the determination of formate (4, 25) and oxalate (26) in stopped assays have also been used. The detection of  $\text{CO}_2$  by manometry provides a continuous assay (3), but this is insensitive and nonspecific. In principle, real-time monitoring could be achieved using a pH-stat system, but this also suffers from not being specific. The consumption of oxalate can also be monitored by the loss of absorbance at 220–230 nm (25), but specificity is again a problem. Many of the above assays could also be used to monitor oxalate oxidase activity. However, the advantage with this enzyme is that it forms  $\text{CO}_2$  and hydrogen peroxide from oxalate and dioxygen. Hydrogen peroxide is easily detected by coupling its production to the oxidation of a dye using a peroxidase (27), and dioxygen consumption could be detected using an oxygen electrode (28). Nevertheless, no single reported assay is continuous, specific, and able to discriminate between the two oxalate-degrading enzymes.

We now report the first real-time and simultaneous monitoring of the consumption of oxalate and formation of  $\text{CO}_2$  and/or formate by oxalate-degrading enzymes that was also capable of distinguishing between decarboxylases and oxidases. This method took advantage of the characteristic infrared absorptions of each of the species involved and, in addition, could identify the C-hydron of formate enabling the mechanistic questions described above to be addressed.

## MATERIALS AND METHODS

**General.** All materials and biochemicals were of the highest grade available and, unless otherwise stated, were purchased from Sigma-Aldrich. Protein concentration was determined using the Pierce Coomassie Plus-200 assay. [ $^{13}\text{C}$ ]Oxalic acid was purchased from Argo International Ltd. (Essex, U.K.) and converted to the sodium salt.  $\text{D}_2\text{O}$  was purchased from Goss Scientific Instruments (Essex, U.K.).

**Enzyme Preparation.** C-Terminally His-tagged *Bacillus subtilis* OxdC was expressed in *Escherichia coli* and purified as described previously (18) with a minor modification. Prior to induction of protein expression the *E. coli* cells were heat treated at 42 °C for 18 rather than 2 min. The yield and specific activity of the enzyme were higher presumably because of the heat-induced expression of more endogenous chaperones to aid protein folding. Buffer exchange of purified OxdC into  $\text{D}_2\text{O}$  buffers was achieved by repeated dilution and concentration cycles using an Amicon Ultra centrifugal filter device (Millipore) over a period of up to 2 h. The pD of  $\text{D}_2\text{O}$  buffers was measured using a pH probe calibrated with  $\text{H}_2\text{O}$  standards and was adjusted with the addition of concentrated DCl. This value will henceforth be called pH because no correction by 0.4 unit was made. Enzyme kinetic

data were obtained with freshly prepared protein. Enzyme concentrations refer to subunit and therefore active site concentrations.

**Stopped Enzyme Assay.** One unit of enzyme activity is defined as the conversion of 1  $\mu\text{mol}$  of substrate to product per minute. Unless otherwise stated, assays contained 1–150 mM potassium oxalate, air-saturated 50 mM sodium citrate, pH 4.0, 200 mM NaCl, 300  $\mu\text{M}$  *o*-phenylenediamine, 10  $\mu\text{M}$  bovine serum albumin, and enzyme (10–20  $\mu\text{g mL}^{-1}$ ) and were incubated for 10 min at 26 °C. Reactions were stopped with the addition of 160 mM dipotassium hydrogen orthophosphate, pH 9.5. The amount of formate produced was determined spectrophotometrically from the reduction of  $\text{NAD}^+$  by formate dehydrogenase as described previously (6).

**Fourier Transform Infrared (FTIR) Spectroscopy.** Stopped-flow FTIR experiments were performed using a Bruker IFS 66/S spectrometer (Bruker UK Ltd.) as described previously (29) with air-saturated solutions. The path length of the  $\text{CaF}_2$  infrared cell was calibrated to be 33  $\mu\text{m}$  by fringe pattern analysis. The temperature of the infrared cell was kept constant at 25 °C. Typically, the instrument collected data across a range of 1000–4000  $\text{cm}^{-1}$  with a time resolution of at least 25 ms per spectrum. The data shown have had control spectra with buffer only subtracted from them. Michaelis–Menten constants were determined using oxalate concentrations between 0 and 25 mM, and data were fitted using the Pharmacology-Simple Ligand Binding-One Site Saturation option in SigmaPlot v8.0.

**EPR Spectroscopy.** X-band EPR spectra were recorded on a modified Bruker ER 200 D-SCR spectrometer (Bruker Spectrospin), fitted with an ESR-900 liquid helium flow cryostat (Oxford Instruments), and run with Bruker software on a Bruker ESP 1600 computer. Conditions were adjusted to ensure nonsaturation of signals. Spectra were obtained with a microwave frequency of 9.44 GHz and power of 2 mW with a receiver gain of 60 at 30 K.

**Computational Chemistry.** The heats of formation, charge densities, spin densities, and ionization potentials of formic acid-derived species in the gas phase at 298 K were calculated using the semiempirical quantum mechanical MOPAC 2000 v1.11 Pro functionality of CambridgeSoft Chem3D Ultra v8.0.3 (Cambridge, MA) using the AM1 (30) potential function with open shell UHF calculations and Wang–Ford charges assuming doublet ground states for odd-electron systems.

## RESULTS

**Choice of Buffer.** To make the initial assignment of the FTIR spectra more straightforward, the absorbance of buffer species in the carboxylate region needed to be minimized. The stopped assay mixture for OxdC is typically buffered with a carboxylic acid such as citrate between pH 4.0 and pH 5.0. Alternative buffers were screened using the stopped assay, and although the specific activity of the enzyme was only 36% in 200 mM pyrophosphate buffer at pH 5.0 compared with the equivalent citrate buffer, it was suitable for the initial studies. Cacodylate was not appropriate because it appeared to react with oxalate directly.

**OxdC Reaction in  $\text{H}_2\text{O}$ .** Using pyrophosphate buffer, it was possible to observe the consumption of oxalate by OxdC

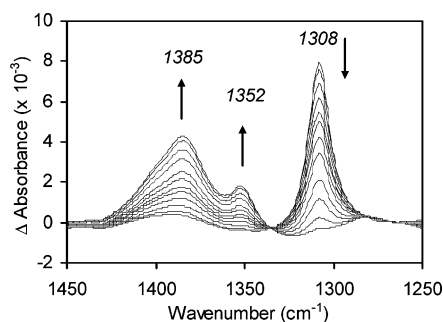


FIGURE 2: Oxalate and formate FTIR spectra of the OxdC reaction in  $\text{H}_2\text{O}$ . The reaction mixture contained oxalate (10 mM after mixing), OxdC (4.5  $\mu\text{M}$ ), and 50 mM pyrophosphate, pH 5.0. Spectra were recorded over a period of 5 min. Arrows indicate the loss of oxalate (1308  $\text{cm}^{-1}$ ) and the appearance of formate (1385 and 1352  $\text{cm}^{-1}$ ) and carbonate (1385  $\text{cm}^{-1}$ ). There is an isosbestic point at 1335  $\text{cm}^{-1}$ .

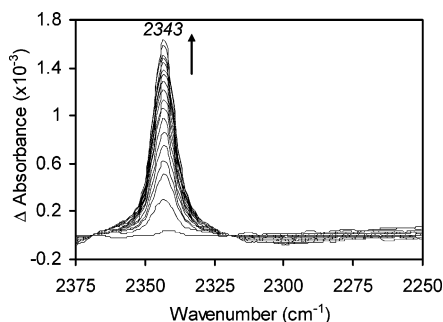


FIGURE 3:  $^{12}\text{CO}_2$  FTIR spectra of the OxdC reaction in  $\text{H}_2\text{O}$ . The reaction mixture contained oxalate (10 mM after mixing), OxdC (4.5  $\mu\text{M}$ ), and 50 mM pyrophosphate, pH 5.0. Spectra were recorded over a period of 5 min. The arrow indicates the appearance of  $^{12}\text{CO}_2$  (2343  $\text{cm}^{-1}$ ).

in real time by monitoring the decrease in absorbance at 1308 (symmetric  $\text{CO}_2$  stretch)  $\text{cm}^{-1}$  (Figure 2). This frequency is consistent with published values (31). Concomitant with the consumption of oxalate was the formation of formate as indicated by the new peaks at 1385 (CH in-plane bend) and 1352 (symmetric  $\text{CO}_2$  stretch)  $\text{cm}^{-1}$ , consistent with known values (32, 33). Carbonate appeared to be partly responsible for the 1385  $\text{cm}^{-1}$  peak because it was greater in intensity than the 1352  $\text{cm}^{-1}$  peak and it is known to give rise to a peak between 1365 and 1390  $\text{cm}^{-1}$  in  $\text{H}_2\text{O}$ , depending on the pH (34). The formation of carbonate was presumably due to the hydration of the enzyme's coproduct,  $\text{CO}_2$ . It was also possible to observe peaks at 2815 (CH fundamental stretch) and 2733 (first overtone of CH in-plane bend)  $\text{cm}^{-1}$  (data not shown), consistent with known values (35). There was an isosbestic point (1335  $\text{cm}^{-1}$ ) and no sign of other species (Figure 2). Control spectra with oxalate, formate, and carbonate confirmed the assignment of the peaks. In  $\text{H}_2\text{O}$ , the observable windows for FTIR spectroscopy are about 3000–1750 and 1570–1050  $\text{cm}^{-1}$ . This precluded the unhindered observation under these conditions of the asymmetric  $\text{CO}_2$  stretches expected for oxalate and formate. Nevertheless, careful subtraction of controls allowed the observation of bands at  $\sim 1571$  and  $\sim 1576$   $\text{cm}^{-1}$  for oxalate and formate, respectively (data not shown).

The observable window at high wavenumbers in  $\text{H}_2\text{O}$  provided the opportunity to observe the formation of  $\text{CO}_2$  during the OxdC reaction. Figure 3 shows the formation of  $\text{CO}_2$  at 2343  $\text{cm}^{-1}$  (asymmetric CO stretch), which was

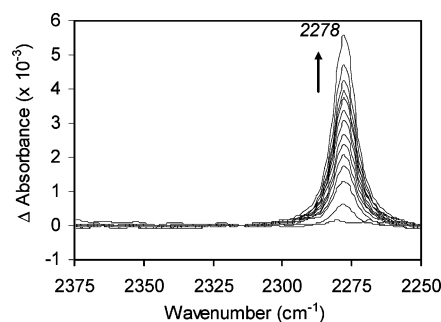


FIGURE 4:  $^{13}\text{CO}_2$  FTIR spectra of the OxdC reaction in  $\text{H}_2\text{O}$ . The reaction mixture contained  $^{13}\text{C}$ oxalate (10 mM after mixing), OxdC (4.5  $\mu\text{M}$ ), and 50 mM pyrophosphate, pH 5.0. Spectra were recorded over a period of 5 min. The arrow indicates the appearance of  $^{13}\text{CO}_2$  (2278  $\text{cm}^{-1}$ ).

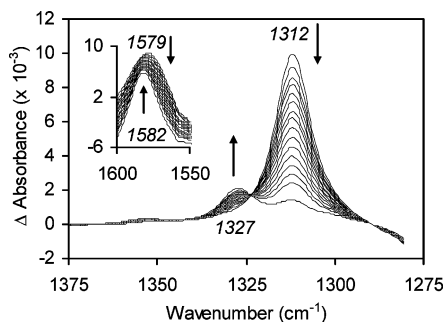


FIGURE 5: Oxalate and formate FTIR spectra of the OxdC reaction in  $\text{D}_2\text{O}$ . The reaction mixture contained oxalate (10 mM after mixing), OxdC (4.5  $\mu\text{M}$ ), and 50 mM pyrophosphate, pH 5.0. Spectra were recorded over a period of 5 min. Arrows indicate the loss of oxalate [1579 (inset) and 1312  $\text{cm}^{-1}$ ] and the appearance of formate [1582 (inset) and 1327  $\text{cm}^{-1}$ ]. There is an isosbestic point at 1324  $\text{cm}^{-1}$ .

essentially concomitant with formate production. The fact that the assay uses a closed cell, coupled with a solubility of  $\text{CO}_2$  under these conditions of 32 mM (36), prevents any escape or gassing out of this product during detection. When using  $^{13}\text{C}$ oxalate as the substrate, the peaks from the substrates and products were shifted to lower wavenumbers as expected ( $^{13}\text{CO}_2$  peak shown in Figure 4). The values were oxalate 1308  $\rightarrow$  1286 [–22 observed, literature values –21 (37) and –20 (38)], formate 1385  $\rightarrow$  1383 and 1352  $\rightarrow$  1330 [–2 and –22 observed, literature values –3 and –20 (32) –2 and –23 (33)], and  $\text{CO}_2$  2343  $\rightarrow$  2278 [–65 observed, literature value –66 (39)]  $\text{cm}^{-1}$ . These shifts further confirmed the assignment of the peaks.

**OxdC Reaction in  $\text{D}_2\text{O}$ .** When the OxdC reaction was monitored in real time by FTIR in  $\text{D}_2\text{O}$  (Figure 5), the disappearance of the oxalate peak was observed at a wavenumber (1312  $\text{cm}^{-1}$ ) similar to that in  $\text{H}_2\text{O}$  (1308  $\text{cm}^{-1}$ ; Figure 2). The observable window in the FTIR spectrum using  $\text{D}_2\text{O}$  is about 2250–1250  $\text{cm}^{-1}$ . Therefore, it was also possible to observe the consumption of oxalate by monitoring the decrease in absorbance at 1579 (asymmetric  $\text{CO}_2$  stretch)  $\text{cm}^{-1}$  (Figure 5, inset). This frequency was again consistent with published values (31). There was a concomitant production of C-deuterio formate, rather than formate, giving new peaks at 1582 (asymmetric  $\text{CO}_2$  stretch) and 1327 (symmetric  $\text{CO}_2$  stretch)  $\text{cm}^{-1}$ . The asymmetric  $\text{CO}_2$  stretch peak width at half-height narrowed from 37 to 24  $\text{cm}^{-1}$  when oxalate was converted to formate (Figure 5, inset). The isomeric shift of the symmetric  $\text{CO}_2$  stretch in C-deuterio



formate was  $-25$ , consistent with a published value of  $-29$  (40). It was also possible to observe formate peaks at  $2115$  (CD fundamental stretch) and  $2025$  (first overtone of CD in-plane bend)  $\text{cm}^{-1}$  (data not shown), giving shifts of  $-700$  and  $-708$ , consistent with known values of  $-699$  and  $-699$  (40). Carbonate did not give rise to peaks in  $\text{D}_2\text{O}$  in the spectral region shown in Figure 5. Control spectra with oxalate and *C*-deuterio formate confirmed the assignment of the peaks. There were no other obvious species observed, and there was an isosbestic point at  $1324 \text{ cm}^{-1}$ . The formation of *C*-deuterio formate showed that the source of the *C*-hydron was solvent as expected.

The concomitant conversion of oxalate to *C*-deuterio formate in  $\text{D}_2\text{O}$  was again observed with  $160 \mu\text{M}$  enzyme and  $700 \mu\text{M}$  oxalate (concentrations after mixing) using  $50 \text{ mM}$  citrate,  $\text{pH } 4.0$ , containing  $200 \text{ mM}$  NaCl and  $20\%$  deuterioglycerol. No enzyme-bound catalytic intermediates were observed. However, at this concentration of enzyme, it was not possible to rule out the presence of such species due to the detection limit of the instrument ( $\sim 300 \mu\text{M}$  oxalate for the  $1312 \text{ cm}^{-1}$  peak). The limited solubility of the enzyme precluded single turnover experiments with saturating substrate (vide infra). The concentration of enzyme used in this experiment was only attainable with the addition of the NaCl and glycerol, which, in the stopped assay, had little effect on catalytic activity. Higher salt concentrations were inhibitory.

**Solvent Deuterium Kinetic Isotope Effect.** It was possible to quantify the rate of reaction using the real-time FTIR spectrophotometric assay. The extinction coefficient of the substrate ( $255 \text{ M}^{-1} \text{ cm}^{-1}$ ) was based on the maximum absorbance of the  $\sim 1310 \text{ cm}^{-1}$  peak at the start of the reactions and confirmed by control reactions without enzyme. This region was chosen because the substrate and product peaks were well separated. The solutions were buffered at the optimum  $\text{pH } 4.0$  (vide infra) with  $50 \text{ mM}$  citrate. NaCl ( $200 \text{ mM}$ ) was again added to increase the solubility of the enzyme. Although citrate absorbed more strongly in the FTIR spectra than pyrophosphate, it was possible to subtract buffer control spectra successfully in the  $1400\text{--}1300 \text{ cm}^{-1}$  region. Nevertheless, the rate of change could be quantified without such subtractions.

Using the conventional stopped assay, the  $K_m$  for oxalate was determined to be  $3.2 \pm 0.5 \text{ mM}$  and the  $V_{\text{max}}$   $134 \pm 6 \text{ units mg}^{-1}$ . Using the FTIR spectrophotometric method with  $50 \text{ mM}$  citrate,  $\text{pH } 4.0$ , containing  $200 \text{ mM}$  NaCl in  $\text{H}_2\text{O}$ , a slightly lower value of  $V_{\text{max}}$  was obtained ( $120 \pm 2 \text{ units mg}^{-1}$ ), but the value of  $K_m$  was somewhat lower ( $0.85 \pm 0.05 \text{ mM}$ ), giving a  $k_{\text{cat}}/K_m$  of  $105 \pm 6 \text{ mM}^{-1} \text{ s}^{-1}$ . The difference in the values could be due to the fact that true initial rates are measured using the FTIR spectrophotometric assay rather than an estimate based on a 10 min time point measurement. The values using the FTIR spectrophotometric method with  $\text{D}_2\text{O}$  were all lower than the corresponding values with  $\text{H}_2\text{O}$ ;  $K_m = 0.22 \pm 0.05 \text{ mM}$ ,  $V_{\text{max}} = 17.0 \pm 0.6 \text{ units mg}^{-1}$ , and  $k_{\text{cat}}/K_m = 57 \pm 13 \text{ mM}^{-1} \text{ s}^{-1}$ . These studies revealed solvent deuterium kinetic isotope effects of  $7.1 \pm 0.3$ ,  $3.9 \pm 0.9$ , and  $1.8 \pm 0.4$  on  $V_{\text{max}}$ ,  $K_m$ , and  $k_{\text{cat}}/K_m$ , respectively.

**Dependence on pH and  $\text{O}_2$ .** The FTIR spectrophotometric assay was also used to determine the pH optimum of the OxdC reaction. This was done using citrate buffer, and

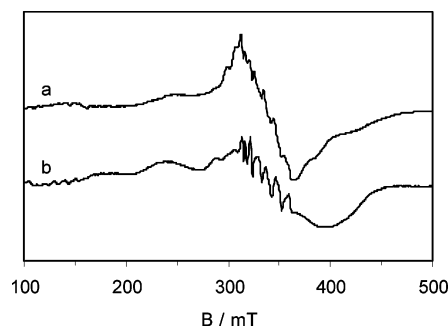


FIGURE 6: X-band EPR spectra of OxdC with and without formate in air-saturated buffer. EPR spectra of OxdC ( $224 \mu\text{M}$ ) in air-saturated  $50 \text{ mM}$  citrate,  $\text{pH } 4.0$ , containing  $20\%$  glycerol and  $200 \text{ mM}$  NaCl are shown (a) as isolated and (b) with  $200 \text{ mM}$  formate.

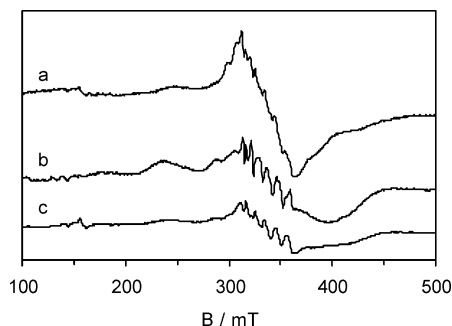
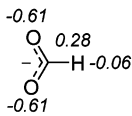
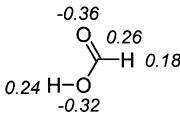
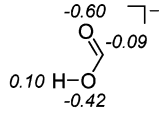
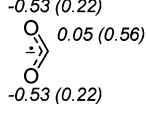
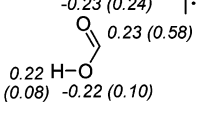
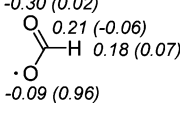
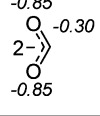


FIGURE 7: X-band EPR spectra of OxdC with and without formate or oxalate in anaerobic buffer. EPR spectra of OxdC ( $246 \mu\text{M}$ ) in air-saturated  $50 \text{ mM}$  citrate,  $\text{pH } 4.0$ , containing  $20\%$  glycerol and  $200 \text{ mM}$  NaCl are shown (a) as isolated, (b) with  $200 \text{ mM}$  formate, and (c) with  $200 \text{ mM}$  oxalate.

maximum activity was observed between  $\text{pH } 3.5$  and  $\text{pH } 4.0$ . This agreed well with values already published ( $\text{pH } 3\text{--}5$ ) (11, 14). In addition, when the assay solutions were preincubated with glucose oxidase, glucose, and catalase, only  $12\%$  of the enzyme activity was retained. This is consistent with previous studies showing the dependence of catalysis on  $\text{O}_2$  (6).

**Hydron Exchange in Formate.** The data above showed that the source of the hydron for the production of formate was solvent. The catalytic step responsible for the delivery of this hydron is obviously kinetically accessible during conversion of oxalate. However, it could also be kinetically accessible when formate is incubated with the enzyme. The binding of formate to the active site of the enzyme has already been observed by crystallography (10). However, the enzyme was buffered at  $\text{pH } 8.0$  in this case, a pH at which the enzyme is not active. To determine whether formate can bind to the enzyme under conditions in which the enzyme is active, EPR spectra were obtained in the presence and absence of formate (Figure 6). The perturbation of the Mn(II) EPR spectrum of the enzyme by formate indicates that it binds to the active site under these conditions. Essentially identical spectra were obtained using dioxygen-saturated buffers (data not shown). Under anaerobic conditions, essentially identical spectra were again obtained with formate (Figure 7). Under these conditions it was also possible to obtain a spectrum in the presence of oxalate without turnover, which gave the largest spectral perturbation (Figure 7). Spectral perturbations in the presence of oxalate have previously been observed with OxdC (15) and oxalate oxidase (41).

Table 1: Semiempirical Quantum Mechanical Calculation of Heats of Formation and Ionization Potentials of Formic Acid Derivatives<sup>a</sup>

Compound	Heat of formation (kcal mol <sup>-1</sup> )	Ionisation potential (eV)
	-109 <sup>b</sup>	4
	-97 <sup>c</sup>	12
	-93	3
	-89	2
	-55	10
	-39	12
	77	-6

<sup>a</sup> Numbers in italic type represent net atomic charges, and those in parentheses represent electron spin densities. For comparison, reported experimental values are -107<sup>b</sup> (48) and -91<sup>c</sup> kcal mol<sup>-1</sup> (49).

Several attempts were made to observe OxdC-catalyzed hydron exchange in formate. This was done by mixing the enzyme (8–16  $\mu$ M) with *C*-deuterio formate (5–10 mM) buffered with 50 mM citrate, pH 4.0, in the FTIR spectrophotometer overnight. In case citrate inhibited the rate of hydron exchange, the experiment was repeated with 50 mM pyrophosphate buffer, pH 5.0, containing 10% glycerol with 200 mM *C*-deuterio formate and 21  $\mu$ M OxdC over a period of 30 min. A shift of the peaks in the 1400–1300 cm<sup>-1</sup> spectral region would have been expected if exchange had occurred. However, exchange was not detected in any of the conditions tried.

**Oxalate Oxidase Assay.** It was also possible to monitor oxalate oxidase (17) enzyme activity in H<sub>2</sub>O in real time using FTIR spectroscopy. In this case, the consumption of oxalate and concomitant formation of CO<sub>2</sub> and carbonate were observed with no formate production, as expected (data not shown). No additional species were observed.

**Theoretical Calculations.** The properties of formic acid-derived species were estimated using semiempirical quantum mechanical calculations (Table 1). The hypothetical carbanion species **3** was surprisingly stable with substantial sharing

of the charge between the carboxyl oxygens but was obviously not as stable as the preferred oxyanion tautomer **1**. Clearly, the p*K*<sub>a</sub> of the carboxylate oxygen [3.75 (42)] would be lower than that of the carbon atom precluding the formation of **3**. As expected, when both atoms were deprotonated to the dianion **7**, it became relatively unstable with a large positive heat of formation being estimated. Species **4–6** were one electron oxidized. For example, the neutral radical species **5**, with the loss of a hydrogen atom from the carbon atom, was significantly more stable than its tautomer **6**, with the loss of hydrogen from oxygen. This seemed to be because only one oxygen carried essentially all of the spin and therefore almost none of the charge in **6**. In other words, there was little resonance stabilization of this neutral radical. It is species **5** that resembles the Mn-bound formyl radical intermediate predicted in the catalytic cycle of OxdC (Figure 1). The majority of the spin was retained on the carbon atom of **5**. Comparison of the heats of formation of **5** with **3** indicates that the formyl radical is prone to gain an electron, as might be expected for the corresponding formyl radical intermediate of the OxdC catalytic cycle (*vide infra*). Further deprotonation of species **5** gave the radical anion **4**, which was much more stable than the dianion **7** presumably because of the presence of only a single negative charge together with the resonance stabilization of both the charge and the spin in **4**. As expected, the ionization potentials of these species were largely dependent on their net charges and are consistent with the heats of formation. For example, the formyl radical species **5** was less prone to lose an electron than its one electron reduced counterpart **3**.

## DISCUSSION

We have demonstrated the first assay for OxdC that is capable of real-time monitoring of the consumption of oxalate and the formation of formate, CO<sub>2</sub>, and carbonate. This took advantage of the infrared absorbance of the substrate and products, a property rarely exploited for enzyme kinetics in general. The method was used to confirm the properties of the enzyme with regard to pH optimum, dependence on dioxygen, and kinetic constants. The *K*<sub>m</sub> for oxalate determined with this assay was 3.8-fold lower than that obtained from stopped assays, indicating the importance of measuring true initial rates of reaction rather than 10 min time points. There are few other opportunities for real-time assays of this enzyme as discussed above. For example, we have preliminary data to show that a pH-stat-type assay can be used, but this does not yield the information on individual components obtained using the FTIR-based assay. The assignment of the infrared peaks was confirmed by using [<sup>13</sup>C]oxalate and by comparison with literature values. The isotopic shifts varied considerably from compound to compound and from peak to peak because of differences in their vibrational modes (C–O or C–H, stretch or bend, and fundamental or overtone vibration), ionization states, symmetries of combined vibrations, and hydrogen bonding. The specificity of the assay also allowed the differentiation of OxdC and oxalate oxidase activities. This is potentially useful in determining the activity and reaction specificity of mutants of either enzyme. No intermediates were detected during multiple turnover experiments, but this assay could in principle be used to monitor the OxdC reaction during a single turnover as well. However, conditions that allow the

enzyme concentration to be high enough for such an experiment have yet to be established. This FTIR-based method would allow other experiments such as the use of  $^{17}\text{O}$  or  $^{18}\text{O}$  to confirm the observed lack of exchange of O atoms between solvent and catalytic intermediates (14) and rule out the remote possibility of O atom exchange between dioxygen and catalytic intermediates.

It has already been established that there is an isotope-sensitive, reversible rate-limiting step prior to decarboxylation based on  $^{13}\text{C}$  and  $^{18}\text{O}$  isotope effects on  $k_{\text{cat}}/K_{\text{m}}$  (14). These have been interpreted, along with other experimental data, as evidence for a rate-limiting step involving the deprotonation of oxalate coupled with electron transfer prior to decarboxylation (Figure 1). It was possible to use our FTIR assay to measure a substantial deuterium solvent kinetic isotope effect. The effect on  $k_{\text{cat}}/K_{\text{m}}$  indicates a solvent isotope-sensitive, reversible rate-limiting step prior to decarboxylation that is likely to be the same step described above (14). The effect on  $V_{\text{max}}$  was very large at  $7.1 \pm 0.3$ , showing that proton transfer events occur during rate-limiting steps. Large solvent isotope effects of 2.28 (43), 5 (44), and 11 (45), for example, have previously been reported with other enzymes. The magnitude of the effect with OxdC is indeed large enough to imply tunneling events. However, colossal solvent isotope effects of several hundred have been observed in a chemical system involving proton-coupled electron transfer where it is thought that the hydrogen transfer distance is large (46). There are no other proton transfers obviously required before oxalate decarboxylation, so it seems likely that the observed solvent isotope effect is, at least in part, reflecting the proton transfer event during the formation of the oxalate radical. Additional inventory, pD profile, viscosity, and temperature-dependence studies will be required in order to establish how many protons are responsible for the solvent isotope effect and whether tunneling accounts for the large effect on  $V_{\text{max}}$ . These would provide additional evidence for proton-coupled electron transfer in a rate-limiting step leading to the oxalate radical.

The catalytic cycle must involve a step where the carbon atom that will go on to produce the product formate is protonated. This proton is expected to be ultimately derived from solvent. We have shown for the first time that this is indeed the case. The rate-limiting step (14) in the catalytic cycle is thought to be the formation of the oxalate radical species as discussed above (Figure 1). This is followed by an essentially irreversible decarboxylation step to give a formyl radical species. Protonation of this radical intermediate would yield formate, which can dissociate from the enzyme together with dioxygen to give the resting state of the enzyme. It would be expected that the protonation and dissociation events could be reversible. Indeed, our EPR data showed that formate could bind to the Mn(II) of OxdC in conditions in which the enzyme is active. However, the spectral changes associated with formate binding were not dependent on dioxygen concentrations. Therefore, it is possible that although formate can bind, dioxygen may not bind to a significant enough extent to allow appreciable formation of the formyl radical intermediate. The binding of oxalate to Mn(II) is estimated to lower the reduction potential of the Mn(III)/Mn(II) couple by  $-400$  mV (41), thus promoting the binding of dioxygen. It is likely that formate binding elicits a more modest lowering of the

potential because it is a weaker acid. If it were sufficient, however, the formation of the formyl radical species would become possible and could manifest itself in C-hydron exchange with solvent. Although it is possible that the proton acceptor, presumed to be Glu162, could return the very same hydron, the presence of this residue on a known flexible lid makes exchange with solvent likely. Our calculations on the formyl radical species **5**, equivalent to the enzyme-bound intermediate, indicate that it is best viewed as a carbon-centered radical species with little carbanion character. A recent hybrid density functional theory study of the oxalate oxidase active site has come to similar conclusions (47). Therefore, to protonate this species, one would envisage the coupled transfer of an electron from the Mn ion. The relative heats of formation and ionization potentials of the radical **5** and the formate carbanion **3** are consistent with such a process being relatively facile. Nevertheless, one advantage of going through a formyl radical intermediate is the avoidance of a formyl carbanion that is very basic. However, our calculations have indicated that such an enzyme-bound species, equivalent to the carbanion **3**, is not as unstable as one might have envisioned. In the end, the FTIR-based assay was unable to detect any C-hydron exchange in formate in the presence of OxdC. One can conclude that the enzyme-bound formyl radical species is not accessible, either kinetically or more probably thermodynamically, from formate. A theoretical study of the related oxalate oxidase reaction indicates that the protonation of the formyl radical intermediate must be fast in order to avoid a spin transition leading to oxalate oxidation rather than decarboxylation (47). It is therefore likely that the active site of OxdC is primarily adapted to generate an oxalate radical and to present a proton at the right place at the right time (16), with the subsequent catalytic steps being facile in the forward direction only. This means that the production of potentially harmful radical intermediate species is confined to the decarboxylation of oxalate.

## ACKNOWLEDGMENT

We thank Shirley Fairhurst for recording EPR spectra, John Tolland for some FTIR data collection, Marcus Durrant for critical reading of the manuscript, and Silvia Ferretti, Nigel Scrutton, Nigel Richards, and Pieter Dorrestein for helpful discussions.

## REFERENCES

- Begley, T. P., and Ealick, S. E. (2004) Enzymatic reactions involving novel mechanisms of carbanion stabilization, *Curr. Opin. Chem. Biol.* 8, 508–515.
- Svedruzic, D., Jonsson, S., Toyota, C. G., Reinhardt, L. A., Ricagno, S., Linqvist, Y., and Richards, N. G. J. (2005) The enzymes of oxalate metabolism: unexpected structures and mechanisms, *Arch. Biochem. Biophys.* 433, 176–192.
- Shimazono, H. (1955) Oxalic acid decarboxylase, a new enzyme from the mycelium of wood destroying fungi, *J. Biochem.* 42, 321–340.
- Emiliani, E., and Bekes, P. (1964) Enzymatic oxalate decarboxylation in *Aspergillus niger*, *Arch. Biochem. Biophys.* 105, 488–493.
- Lillehoj, E. B., and Smith, F. G. (1965) An oxalic acid decarboxylase of *Myrothecium verrucaria*, *Arch. Biochem. Biophys.* 109, 216–220.
- Tanner, A., Bowater, L., Fairhurst, S. A., and Bornemann, S. (2001) Oxalate decarboxylase requires manganese and dioxygen for activity—overexpression and characterization of *Bacillus subtilis* YvrK and YoaN, *J. Biol. Chem.* 276, 43627–43634.



7. Requena, L., and Bornemann, S. (1999) Barley (*Hordeum vulgare*) oxalate oxidase is a manganese-containing enzyme, *Biochem. J.* 343, 185–190.
8. Khuri, S., Bakker, F. T., and Dunwell, J. M. (2001) Phylogeny, function, and evolution of the cupins, a structurally conserved, functionally diverse superfamily of proteins, *Mol. Biol. Evol.* 18, 593–605.
9. Woo, E. J., Dunwell, J. M., Goodenough, P. W., Marvier, A. C., and Pickersgill, R. W. (2000) Germin is a manganese containing homohexamer with oxalate oxidase and superoxide dismutase activities, *Nat. Struct. Biol.* 7, 1036–1040.
10. Anand, R., Dorrestein, P. C., Kinsland, C., Begley, T. P., and Ealick, S. E. (2002) Structure of oxalate decarboxylase from *Bacillus subtilis* at 1.75 Å resolution, *Biochemistry* 41, 7659–7669.
11. Tanner, A., and Bornemann, S. (2000) *Bacillus subtilis* YvrK is an acid-induced oxalate decarboxylase, *J. Bacteriol.* 182, 5271–5273.
12. Dutton, M. V., and Evans, C. S. (1996) Oxalate production by fungi: its role in pathogenicity and ecology in the soil environment, *Can. J. Microbiol.* 42, 881–895.
13. Dunwell, J. M., Khuri, S., and Gane, P. J. (2000) Microbial relatives of the seed storage proteins of higher plants: conservation of structure and diversification of function during evolution of the cupin superfamily, *Microbiol. Mol. Biol. Rev.* 64, 153–179.
14. Reinhardt, L. A., Svedruzic, D., Chang, C. H., Cleland, W. W., and Richards, N. G. J. (2003) Heavy atom isotope effects on the reaction catalyzed by the oxalate decarboxylase from *Bacillus Subtilis*, *J. Am. Chem. Soc.* 125, 1244–1252.
15. Chang, C. H., Svedruzic, D., Ozarowski, A., Walker, L., Yeagle, G., Britt, R. D., Angerhofer, A., and Richards, N. G. J. (2004) EPR spectroscopic characterization of the manganese center and a free radical in the oxalate decarboxylase reaction—Identification of a tyrosyl radical during turnover, *J. Biol. Chem.* 279, 52840–52849.
16. Chang, C. H., and Richards, N. G. J. (2005) Intrinsic carbon–carbon bond reactivity at the manganese center of oxalate decarboxylase from density functional theory, *J. Chem. Theory Comput.* 1, 994–1007.
17. Escutia, M. R., Bowater, L., Edwards, A., Bottrill, A. R., Burrell, M. R., Polanco, R., Vicuña, R., and Bornemann, S. (2005) Cloning and sequencing of two *Ceriporiopsis subvermisporea* bicupin oxalate oxidase allelic isoforms: implications for the reaction specificity of oxalate oxidases and decarboxylases, *Appl. Environ. Microbiol.* 71, 3608–3616.
18. Just, V. J., Stevenson, C. E. M., Bowater, L., Tanner, A., Lawson, D. M., and Bornemann, S. (2004) A closed conformation of *Bacillus subtilis* oxalate decarboxylase OxdC provides evidence for the true identity of the active site, *J. Biol. Chem.* 279, 19867–19874.
19. Dashek, W. V., and Micales, J. A. (1997) Assay and purification of enzymes—oxalate decarboxylase, in *Methods in Plant Biochemistry and Molecular Biology* (Dashek, W. V., Ed.) pp 49–71, CRC Press, Boca Raton, FL.
20. Magro, P., Marciano, P., and Di Lenna, P. (1988) Enzymatic oxalate decarboxylation in isolates of *Sclerotinia sclerotiorum*, *FEMS Microbiol. Lett.* 49, 49–52.
21. Chiriboga, J. (1962) Radiometric analysis of metals using chelates labeled with carbon-14 and liquid scintillation counting procedures, *Anal. Chem.* 34, 1843.
22. Mehta, A., and Datta, A. (1991) Oxalate decarboxylase from *Collybia velutipes*: purification, characterization, and cDNA cloning, *J. Biol. Chem.* 266, 23548–23553.
23. Dutton, M. V., Kathiara, M., Gallagher, I. M., and Evans, C. S. (1994) Purification and characterization of oxalate decarboxylase from *Coriolus versicolor*, *FEMS Microbiol. Lett.* 116, 321–325.
24. Micales, J. A. (1995) Oxalate decarboxylase in the brown-rot wood decay fungus *Postia placenta*, *Mater. Org.* 29, 177–186.
25. Shimazono, H., and Hayaishi, O. (1957) Enzymatic decarboxylation of oxalic acid, *J. Biol. Chem.* 227, 151–159.
26. Sharma, S., Nath, R., and Thind, S. K. (1993) Recent advances in measurement of oxalate in biological materials, *Scanning Microsc.* 7, 431–441.
27. Emiliani, E., and Riera, B. (1968) Enzymatic oxalate decarboxylation in *Aspergillus niger*: II. Hydrogen peroxide formation and other characteristics of the oxalate decarboxylase, *Biochim. Biophys. Acta* 167, 414–421.
28. Bowater, L., Fairhurst, S. A., Just, V. J., and Bornemann, S. (2004) *Bacillus subtilis* YxaG is a novel Fe-containing quercetin 2,3-dioxygenase, *FEBS Lett.* 557, 45–48.
29. George, S. J., Allen, J. W. A., Ferguson, S. J., and Thorneley, R. N. F. (2000) Time-resolved infrared spectroscopy reveals a stable ferric heme-NO intermediate in the reaction of *Paracoccus pantotrophus* cytochrome cd(1) nitrite reductase with nitrite, *J. Biol. Chem.* 275, 33231–33237.
30. Dewar, M. J. S., Zoebisch, E. G., Healy, E. F., and Stewart, J. J. P. (1985) The development and use of quantum mechanical molecular models 76. AM1—a new general purpose quantum mechanical molecular model, *J. Am. Chem. Soc.* 107, 3902–3909.
31. Shippey, T. A. (1980) Vibrational studies of anhydrous lithium, sodium and potassium oxalates, *J. Mol. Struct.* 67, 223–233.
32. Hudson, R. L., and Moore, M. H. (2000) IR spectra of irradiated cometary ice analogues containing methanol: a new assignment, a reassignment, and a nonassignment, *Icarus* 145, 661–663.
33. Iwaki, M., and Rich, P. R. (2004) Direct detection of formate ligation in cytochrome C oxidase by ATR-FTIR spectroscopy, *J. Am. Chem. Soc.* 126, 2386–2389.
34. Wijnja, H., and Schulthess, C. P. (1999) ATR-FTIR and DRIFT spectroscopy of carbonate species at the aged  $\gamma$ -Al<sub>2</sub>O<sub>3</sub>/water interface, *Spectrochim. Acta* 55A, 861–872.
35. Mentzen, B. F., and Oddo, Y. (1980) Coordination chemistry in anhydrous monovalent metallic formates. I. The crystal structure of anhydrous potassium formate KHCOO. C<sub>2h</sub>-octahedral eight-coordinate of the potassium atom, *Inorg. Chim. Acta* 43, 237–241.
36. Dean, J. A. (1992) *Lange's Handbook of Chemistry*, 14th ed., McGraw-Hill, New York.
37. Clark, R. J. H., and Firth, S. (2002) Raman, infrared and force field studies of K<sub>2</sub><sup>13</sup>C<sub>2</sub>O<sub>4</sub>·H<sub>2</sub>O and K<sub>2</sub><sup>13</sup>C<sub>2</sub>O<sub>4</sub>·H<sub>2</sub>O in the solid state and in aqueous solution, and of (NH<sub>4</sub>)<sub>2</sub><sup>13</sup>C<sub>2</sub>O<sub>4</sub>·H<sub>2</sub>O and (NH<sub>4</sub>)<sub>2</sub><sup>13</sup>C<sub>2</sub>O<sub>4</sub>·H<sub>2</sub>O in the solid state, *Spectrochim. Acta* 58A, 1731–1746.
38. Jones, D. P., and Griffith, W. P. (1980) Studies on the vibrational spectra of perhydrates-I. Spectra of normal and isotopically substituted (<sup>2</sup>H, <sup>13</sup>C) alkali metal oxalate perhydrates, M<sub>2</sub>C<sub>2</sub>O<sub>4</sub>·H<sub>2</sub>O<sub>2</sub>, *Spectrochim. Acta* 36A, 375–378.
39. Schriver, A., Schriver-Mazzuoli, L., and Vigasin, A. A. (2000) Matrix isolation spectra of the carbon dioxide monomer and dimer revisited, *Vib. Spectrosc.* 23, 83–94.
40. Spinner, E., and Rowe, J. E. (1979) Effects of isotopic dilution on the infrared spectrum of solid sodium formate, *Aust. J. Chem.* 32, 481–501.
41. Whittaker, M. M., and Whittaker, J. W. (2002) Characterization of recombinant barley oxalate oxidase expressed by *Pichia pastoris*, *J. Biol. Inorg. Chem.* 7, 136–145.
42. Dawson, R. M. C., Elliott, D. C., Elliott, W. H., and Jones, K. M. (1969) in *Data for Biochemical Research*, Oxford University Press, Oxford.
43. Basran, J., Harris, R. J., Sutcliffe, M. J., and Scrutton, N. S. (2003) H-tunneling in the multiple H-transfers of the catalytic cycle of morphinone reductase and in the reductive half-reaction of the homologous pentaerythritol tetranitrate reductase, *J. Biol. Chem.* 278, 43973–43982.
44. Politicelli, F., Basran, J., Faso, C., Cona, A., Minervini, G., Angelini, R., Federico, R., Scrutton, N. S., and Tavladoraki, P. (2005) Lys300 plays a major role in the catalytic mechanism of maize polyamine oxidase, *Biochemistry* 44, 16108–16120.
45. Klimacek, M., and Nidetzky, B. (2002) A catalytic consensus motif for D-mannitol 2-dehydrogenase, a member of a polyol-specific long-chain dehydrogenase family, revealed by kinetic characterization of site-directed mutants of the enzyme from *Pseudomonas fluorescens*, *Biochem. J.* 367, 13–18.
46. Huynh, M. H. V., and Meyer, T. J. (2004) Colossal kinetic isotope effects in proton-coupled electron transfer, *Proc. Natl. Acad. Sci. U.S.A.* 101, 13138–13141.
47. Borowski, T., Bassan, A., Richards, N. G. J., and Siegbahn, P. E. M. (2005) Catalytic reaction mechanism of oxalate oxidase (germin). A hybrid DFT study, *J. Chem. Theory Comput.* 1, 686–693.
48. Bartmess, J. E., and McIver, R. T. (1979) *Gas-Phase Ion Chemistry*, Vol. II, Academic Press, New York.
49. Cox, J. O., and Pilcher, G. (1970) *Thermochemistry of Organic and Organometallic Compounds*, Academic Press, New York.